

Phonon enhanced inverse population in asymmetric double quantum wells

Michael A. Stroscio

U.S. Army Research Office, P.O. Box 12211, Research Triangle Park, North Carolina 27709-2211

Mikhail Kisin,^{a)} Gregory Belenky, and Serge Luryi

Department of Electrical and Computer Engineering, State University of New York at Stony Brook, New York 11794-2350

(Received 26 July 1999; accepted for publication 24 September 1999)

Interwell optical-phonon-assisted transitions are studied in an asymmetric double-quantum-well heterostructure comprising one narrow and one wide coupled quantum wells (QWs). We show that the depopulation rate of the lower subband states in the narrow QW can be significantly enhanced thus facilitating the intersubband inverse population, if the depopulated subband is aligned with the second subband of the wider QW, while the energy separation from the first subband is tuned to the highest energy optical-phonon mode. © 1999 American Institute of Physics.

[S0003-6951(99)03447-6]

The operation of intersubband lasers requires fast depopulation of the final states for light-emitting transitions. In A_3B_5 -based heterostructures the longitudinal-optical (LO) phonon-assisted interwell electronic transitions provide the most effective depopulation mechanism for the lower subband electron states of the active quantum well (QW).¹ Recently this approach has been successfully implemented in design of intersubband injection lasers, both cascaded^{2,3} and noncascaded.⁴ In the simplest case, the unit cell of the device includes two coupled QWs, *A* and *B*, as in Fig. 1, specially designed to ensure fast depopulation of the lower level *A1* of the active QW *A*. The depopulation time, τ_{out} , must be shorter than the characteristic time, τ_{21} , for intersubband *A2*–*A1* nonradiative relaxation.^{2–4} The relationship $\tau_{out} \ll \tau_{21}$ thus controls the population inversion between levels *A2* and *A1* involved in the light-emitting transition. Both the interwell (τ_{out})_{AB} and intrawell ($\tau_{21}, \tau_{11}, \tau_{22}$)_{AA} transitions in A_3B_5 -based heterostructures are basically caused by similar LO-phonon emission events. The rates for different processes depend on the value of the phonon wave vector, *q*, involved in the transition, as well as on the electron-phonon overlap integral. The Fröhlich matrix element for LO-phonon scattering contains a $1/q^2$ dependence, so traditionally, the energy separation $E_{A1,B1}$ between the lowest level of the active QW *A* and the lowest (drain) level of the adjacent QW *B* is made resonant with the emitted phonon quantum, $\hbar\omega_{ph}$. This ensures that the interwell depopulation process is efficiently mediated by long-wavelength phonons.² However, even under the resonant condition, the relationship $\tau_{out} \ll \tau_{21}$ is difficult to fulfill without severe limitations. First, one needs a sufficiently large *A2*–*A1* energy separation which ensures slow intrawell intersubband relaxation owing to the large transferred momentum *q*. However, even for $E_{A2,A1} \geq 100$ meV, emptying of the upper lasing subband via LO-phonon emission processes occurs on a fast time scale of about 1–3 ps. Another limitation arises due to the small wave-function overlap of the initial and final electron states in interwell transitions. Even for the resonant electron-

phonon scattering this leads to a depopulation time τ_{out} on the scale of 0.5–1.5 ps. As a result, the typical values for intrawell relaxation and interwell depopulation times in A_3B_5 -based heterostructures are comparable, hence strong intersubband population inversion is difficult to achieve.

It is worth noting that a much shorter relaxation time $\tau_{11} \approx 0.1$ ps is seen in intrasubband LO-phonon scattering processes.^{5–7} This can be traced to both the strong overlap integral for initial and final electron states in the same QW and to the relatively small transferred phonon momentum.

In this work, we propose a depopulation process, which combines the advantages of the small momentum transfer in the intersubband electron-phonon resonance with the substantial wave-function overlap characteristic of the intrasubband scattering. In contrast to the traditional design of injection intersubband lasers,^{2–4} this approach assumes the adjacent QW to be wider than the active QW of the laser heterostructure. The depopulated level *A1* should be aligned then with the second subband of the adjacent QW, *B2*, and, at the same time, the energy separation $E_{B2,B1}$ is adjusted to

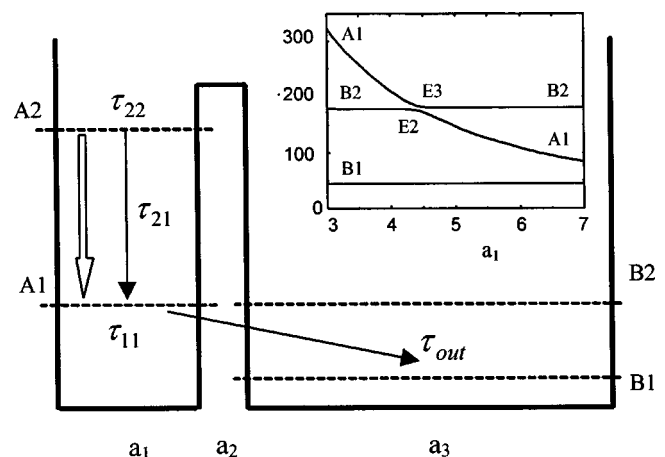


FIG. 1. Model band diagram and energy levels of an AlAs/GaAs double quantum well heterostructure. Double-lined arrow corresponds to the light-emitting transition in the heterostructure. The inset shows the positions of three lowest subbands (in meV) as a function of the narrow well width a_1 (in nm) for fixed values $a_2 = 2$ nm and $a_3 = 10$ nm.

^{a)}Electronic mail: mvk@ee.sunysb.edu

the emitted optical-phonon quantum, $\hbar\omega_{\text{ph}}$. We show that the depopulation rate in this *double resonance* can be significantly enhanced, thus facilitating the intersubband inverse population in the active QW. We also show that this type of resonance features a single-peak behavior despite the strong dispersion of LO-phonon modes due to the optical-phonon confinement effect.

The energy levels for the double QW AlAs–GaAs heterostructure have been calculated in the effective-mass approximation, neglecting nonparabolicity. For simplicity, the outer barriers have been assumed infinite, but the finite barrier height between the QWs has been taken into account. This model is reasonable because the wave functions of the initial and final electron states in the depopulation process, ψ_{A1} and ψ_{B1} , overlap mostly inside the heterostructure. The inset to Fig. 1 shows the subband levels calculated under the flatbands condition as a function of the narrow well width a_1 . The width of the wider well, a_3 , and the barrier layer width, a_2 , are kept constant, so we can change the lowest subband energy separation, $E_{A1,B1}$, by varying a_1 . The transition rates will also be plotted as a function of the narrow well width a_1 , since such a representation depends only slightly on the initial kinetic energy of the electron. Note that the initial electron states in the narrow well A belong to the second subband of the heterostructure, E_2 , only if the width of this well is larger than a critical value $a_{1c} \approx 0.5a_3$, corresponding to the anticrossing of levels $A1$ and $B2$, i.e., for $a_{1c} < a_1 < a_3$. After the crossover, when $a_1 < a_{1c}$, the initial electron states for the interwell transitions belong to the third subband of the heterostructure, E_3 , since the electron wave functions of the second subband are now mostly localized in the wider well B .

To make the physical picture clearer, we consider here only the transitions from the $A1$ -subband bottom associated with the optical-phonon emission. In thin-layer heterostructures the optical phonon confinement effect leads to a rich variety of modes and significantly influences the electron-phonon scattering rates.⁶ We include this effect in our calculations. In Fig. 2 we compare the total transition rate by all confined and interface optical-phonon modes, τ_{out}^{-1} , with the results obtained by using the single-mode bulk-phonon spectrum approximation. The standard Fermi's golden rule formulation was used in both cases. In accordance with the sum rule,^{5,7} the total rate falls in the interval defined by the interaction with bulk well-type phonons, $\hbar\omega_{\text{LO}}^{\text{GaAs}}$, and bulk barrier-type phonons, $\hbar\omega_{\text{LO}}^{\text{AlAs}}$, except near the onset of resonant electron-phonon scattering, where the interwell transition rate is very sensitive to the phonon spectrum dispersion. Confined phonon modes in the QW layers, $\omega_{\text{ph}} = \omega_{\text{LO}}^{\text{GaAs}}$, are dominant at the onset of the resonance, while the outer- and inner-interface antisymmetric phonon modes with frequencies in the Reststrahlen band of the barrier semiconductor material, $\omega_{\text{TO}}^{\text{AlAs}} < \omega_{\text{ph}} < \omega_{\text{LO}}^{\text{AlAs}}$, are primarily responsible for the next two step-like increases of the interwell scattering rate. One can see that the optical-phonon confinement tends to diminish the peak rate value both at the well- and barrier-type phonon-emission thresholds, spreading the oscillator strength among the different phonon modes.

The rapid increase of the transition rates at the smaller values of a_1 in Fig. 2 corresponds to the onset of another

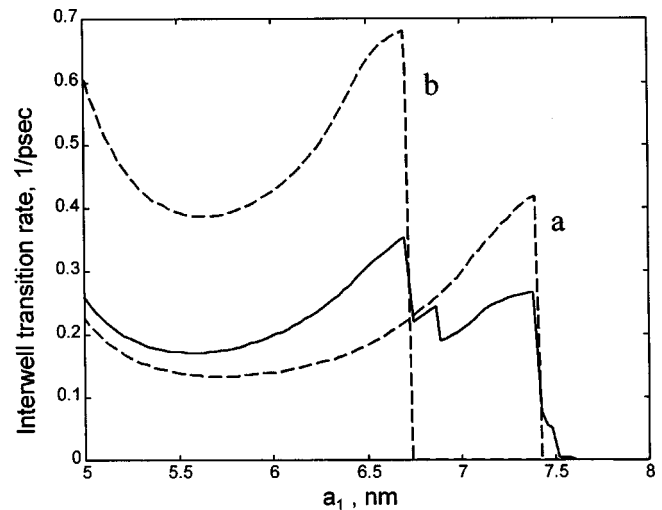


FIG. 2. Onset for the interwell electron-phonon resonance. Solid line shows the total $A1$ – $B1$ transition rate by all confined and interface LO-phonon modes of a double quantum well heterostructure as a function of the narrow well width a_1 . Here $a_2 = 2$ nm and $a_3 = 10$ nm. Two dashed curves represent the interwell transition rates calculated in the single-mode bulk-like LO-phonon spectrum approximation with phonon energies: (a) $\hbar\omega_{\text{LO}}^{\text{GaAs}} = 36$ meV, and (b) $\hbar\omega_{\text{LO}}^{\text{AlAs}} = 51$ meV.

type of resonance—the abrupt enhancement of the electron wave-function overlap and, consequently, the rise of the phonon emission rate due to the resonant penetration of the wave function of the initial electron state $A1$ into the adjacent QW B under the $A1$ – $B2$ anticrossing condition. As mentioned earlier, in the vicinity of this anticrossing there is some ambiguity in determining precise location of the initial electron state for the depopulation process. In intersubband laser heterostructures the lowest level for light-emitting transition is filled mainly by relatively slow nonradiative intersubband transitions. Therefore, for the purpose of this study we can consider the depopulated states as the true energy eigenstates of the double quantum well heterostructure, neglecting the coherent tunneling oscillations.^{8,9} We define a_{1c} as a point where the scattering rate from the lower-energy state $|E_2\rangle \approx (|A_1\rangle + |B_2\rangle)/\sqrt{2}$ equals the scattering rate from the higher-energy state $|E_3\rangle \approx (|A_1\rangle - |B_2\rangle)/\sqrt{2}$. The condition $a_1 = a_{1c}$ thus determines the peak value of the phonon-emission interwell transitions. This new resonance takes place in a very narrow range of a_1 though in the experimental study it can be adjusted by an applied external electric field.¹⁰ It is readily seen that the interwell transition process can be optimized even more, if we can fulfill both the electron-overlap and the phonon-emission resonance conditions, i.e., by setting $a_1 = a_{1c}$ and $E_{A1,B1} = \hbar\omega_{\text{LO}}^{\text{AlAs}}$. In Fig. 3 the latter condition is realized at $a_3 = 18$ nm; we see that the peak rate in this case is highest. When energy separation $E_{A1,B1}$ becomes smaller than $\hbar\omega_{\text{LO}}^{\text{AlAs}}$, the peak rate value decreases (Fig. 3, curve 20) due to the elimination of the high-energy barrier-type interface phonon modes from the emission process and it vanishes abruptly, when no single quantum of any phonon mode matches $E_{A1,B1}$. Although both the interface and the confined optical-phonon modes participate in the double electron-phonon resonance on equal footing (as illustrated by curve 10 in Fig. 3), this resonance reveals a simple one-peak behavior in contrast to the highly dispersed onset for interwell scattering. This is a conse-

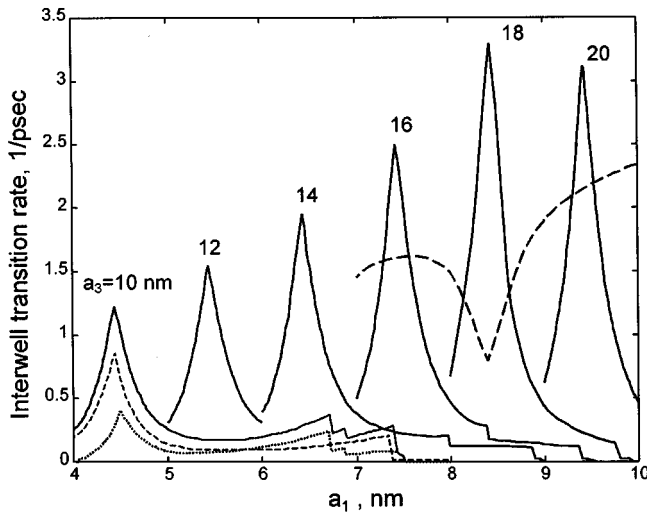


FIG. 3. Peak values of the interwell optical-phonon-assisted transition rate under the double electron-phonon resonance condition. The curves are labeled with the value of the wider quantum well width a_3 in nm. Curve 10 details individual contributions to the overall phonon-emission rate: dashed line-confined phonon modes, dotted line-interface phonon modes. Bold dashed line represents the rate of the nonradiative intrawell intersubband transitions, τ_{21}^{-1} , for the heterostructure with $a_3 = 18$ nm.

quence of the very narrow energy range of $A1-B2$ anticrossing required for the resonant penetration of ψ_{A1} into quantum well B .

The peak value of τ_{out}^{-1} obtained by the proposed process (Fig. 3, curve 18) is one order of magnitude larger than the maximum transition rate at the onset of electron-phonon resonance traditionally employed for the lower level depopulation in intersubband injection lasers. It is also important that the increase of the depopulation rate τ_{out}^{-1} due to the $A1-B2$ anticrossing is accompanied by a simultaneous reduction of the nonradiative $A2-A1$ transition rate, τ_{21}^{-1} . Physically, the intrawell rate decreases for the same reason, namely due to the abrupt reduction of the intrawell electron overlap when $A1$ states penetrate into adjacent QW B at the $A1-B2$ resonance. This process will further increase the population ratio between the levels $A2$ and $A1$. This may enhance the laser action even despite the concomitant decrease of the matrix element for light-emitting transitions. This situation is typical for intersubband lasers with optical transitions indirect in real space.¹¹ The exemplary intrawell $A2-A1$ phonon-emission rate for the heterostructure with $a_3 = 18$ nm is shown in Fig. 3 by the bold dashed line. The total intersubband population ratio, η_{tot} , can be roughly estimated as $\eta_{tot} = n_{A2}/n_{A1} \approx \tau_{21}^{-1}/\tau_{out}^{-1}$ and under the double resonance condition ($a_1 = 8.5$ nm) it is as high as $\eta_{tot} \approx 6$, whereas outside the resonance region the total population inversion disappears. Thus for $a_1 = 8.0$ nm, we have only $\eta_{tot} \approx 0.5$. It is worth noting that the total subband populations determine the optical gain and the output power only in the high electron concentration limit.¹² For low electron concentrations $n_A \leq 10^{11} \text{ cm}^{-2}$, the lasing action is governed by the local nonequilibrium k -space population inversion between $A2$ and $A1$ subband bottoms which cannot be reduced to η_{tot} . In this case, the interwell depopulation rate becomes

even more important. Assuming that $A2$ electrons are distributed in a narrow region near the subband bottom we have^{3,12}

$$\eta_{loc} = \left(\frac{n_{A2}}{n_{A1}} \right)_{k=0} \approx \eta_{tot} \left(1 + \frac{\tau_{11}}{\tau_{out}} \right)^{E_{A2A1}/\hbar\omega_{ph}}$$

For a large $A2-A1$ separation and low values of τ_{out} the local population inversion can be significantly enhanced. For the double-quantum-well heterostructure with $a_1 = 8.5$ nm, $a_2 = 2$ nm, and $a_3 = 18$ nm, we find $\tau_{11}/\tau_{out} \approx 0.6$ and $E_{A2A1}/\hbar\omega_{LO}^{GaAs} \approx 5$, which results in $\eta_{loc} \approx 10\eta_{tot}$ and may be very favorable for the overall laser performance.

It should be clearly understood, however, that population inversion is not the only important parameter for a successful laser design. For instance, care must be taken to minimize the leakage of electrons from the upper lasing level $A2$ through a third energy level $B3$ of the wide well, which shunts the useful injection current. This process has little effect on the population inversion but it increases the lasing threshold. For our exemplary heterostructure, calculations show that the level $B3$ can be located within less than one $\hbar\omega_{ph}$ from the level $A2$, thus suppressing phonon-assisted leakage, by taking the active quantum well width $a_1 \approx 11.5$ nm and applying an external electric field 8 kV/cm to satisfy the double electron-phonon resonance condition.

In summary we have shown that the depopulation rate of the lower lasing level and hence the inverse population ratio in the active QW of a double quantum well intersubband laser heterostructure can be enhanced by an order of magnitude if the condition of the electron-phonon resonance for the depopulation process is accompanied by the anticrossing between the depopulated level in active QW and the second energy level in an adjacent wide well.

This work was supported by the U.S. Army Research Office.

- ¹D. Y. Oberli, J. Shah, T. C. Damen, J. M. Kuo, and J. E. Henry, Appl. Phys. Lett. **56**, 1239 (1998).
- ²J. Faist, F. Capasso, D. L. Sivco, C. Sirtori, A. L. Hutchinson, and A. Y. Cho, Science **264**, 553 (1994); J. Faist, F. Capasso, C. Sirtori, D. L. Sivco, A. L. Hutchinson, and A. Y. Cho, Appl. Phys. Lett. **66**, 538 (1995).
- ³J. Faist, F. Capasso, C. Sirtori, D. L. Sivco, A. L. Hutchinson, M. S. Hybertsen, and A. Y. Cho, Phys. Rev. Lett. **76**, 411 (1996).
- ⁴C. Gmachl, F. Capasso, A. Tredicucci, D. L. Sivco, A. L. Hutchinson, S. N. G. Chu, and A. Y. Cho, Appl. Phys. Lett. **73**, 3830 (1998).
- ⁵H. Rucker, E. Molinari, and P. Lugli, Phys. Rev. B **45**, 6747 (1992).
- ⁶M. A. Stroscio, G. J. Iafrate, K. W. Kim, M. A. Littlejohn, H. Goronkin, and G. N. Maracas, Appl. Phys. Lett. **59**, 1093 (1991); M. Stroscio, J. Appl. Phys. **80**, 6864 (1996).
- ⁷M. V. Kisin, M. A. Stroscio, G. Belenky, V. B. Gorfinkel, and S. Luryi, J. Appl. Phys. **83**, 4816 (1998).
- ⁸T. Matsusue, M. Tsuchiya, J. N. Schulman, and H. Sakaki, Phys. Rev. B **42**, 5719 (1990).
- ⁹S. Luryi, IEEE J. Quantum Electron. **27**, 54 (1991).
- ¹⁰S. Ozaki, J. M. Feng, J. H. Park, S. Osako, H. Kubo, M. Morifuji, N. Mori, and C. Hamaguchi, J. Appl. Phys. **83**, 962 (1998).
- ¹¹J. Faist, F. Capasso, D. L. Sivco, A. L. Hutchinson, C. Sirtori, S. N. F. Chu, and A. Y. Cho, Appl. Phys. Lett. **65**, 2901 (1994); C. Sirtori, A. Tredicucci, F. Capasso, J. Faist, D. L. Sivco, A. L. Hutchinson, and A. Y. Cho, Opt. Lett. **23**, 463 (1998).
- ¹²V. Gorfinkel, S. Luryi, and B. Gelmont, IEEE J. Quantum Electron. **32**, 1995 (1996).